Trace gas oxidation supports sub-surface microbial communities across Namib Desert fog and aridity gradients

Dana Z. Tribbia[1,2], Pedro H. Lebre[3], Xabier Vázquez-Campos[1], Angelique E. Ray[1,4], Thomas Laird[1], Náthali Machado de Lima[1], Gillian Maggs-Kölling[5], Don A. Cowan[3], Belinda C. Ferrari[1,2]#.

[1]*School of Biotechnology and Biomolecular Sciences, UNSW Sydney, NSW, Australia.*

[2]*Evolution and Ecology Research Centre, UNSW Sydney, NSW, Australia.*

[3]*Centre for Microbial Ecology and Genomics, Department of Biochemistry, Genetics and Microbiology, University of Pretoria, Pretoria, South Africa.*

[4]*NASA Ames Research Center, Moffett Field, California, USA.*

[5]*Gobabeb-Namib Research Institute, Walvis Bay, Namibia.*

#Corresponding author: Belinda C. Ferrari, b.ferrari@unsw.edu.au

Keywords

Hydrogen oxidation, drylands, soil, precipitation, hyperarid, microbial resuscitation, chemotrophy, hydro-genesis.

Abstract

Widely accepted climate predictions indicate that drylands will expand to cover more than half of the Earth's terrestrial surface by the end of the 21st century. In these environments, harsh conditions including nutrient and water limitations restrict plant and animal life, thereby increasing the importance of soil microbial communities in nutrient cycling and ecosystem functioning. The Namib Desert is a distinctive dryland ecosystem characterised by a steep natural aridity gradient, transitioning from a coastal hyperarid zone influenced by frequent fog deposition to an inland arid region receiving seasonal rainfall. This study investigates the impact of water availability and moisture regime on microbial trace gas oxidation and community composition across this aridity gradient. Quantitative analyses revealed that total microbial abundance and activity indicators, including ATP concentrations and respiration rates, were significantly ($p < 0.005$) reduced in hyperarid soils compared to their arid counterparts. In contrast, hyperarid fog-dominated soils exhibited significantly ($p < 0.0005$) elevated rates of atmospheric hydrogen oxidation, even in the absence of water inputs. We propose that sustained high-affinity hydrogen oxidation, coupled with rapid microbial resuscitation following wetting events, supports shallow sub-surface microbial communities in the Namib Desert, particularly in the coastal hyperarid zone. Together, these findings challenge current understanding of the lower limits of microbial activity and reveal alternate metabolic pathways that enable microbial persistence in hyperarid hot desert soils.

Importance

Drylands are expanding globally, yet the mechanisms that allow microbial life to persist under extreme and sustained water limitation remain poorly understood. This study demonstrates that atmospheric trace gas oxidation, particularly high-affinity hydrogen oxidation, supports active and resilient microbial communities in hyperarid soils of the Namib Desert, even in the absence of liquid water inputs. By revealing how microbes may

couple trace gas metabolism to energy and water generation, our findings provide new insight into the lower limits of microbial activity in dry hot desert soils and highlight the need to investigate how microbes persist and sustain soil ecosystem functioning.

Introduction

Water availability across a natural xeric gradient in the Namib Desert

The Namib Desert is a distinctive dryland ecosystem situated along a steep natural aridity gradient on the west coast of Namibia [1, 2]. Low intensity rainfall events occur intermittently (< 18 days/year) along this gradient [3, 4]. Precipitation frequency and volume increase progressively from west to east, with the coastal region receiving the lowest average annual rainfall (~10 mm/year) [4]. These sporadic rainfall events are separated by prolonged dry periods, leaving much of the soil sub-surface desiccated for lengthy periods of time [3, 4]. The Aridity Index (AI), defined as the ratio of precipitation to potential evapotranspiration, divides the Namib Desert into two primary zones: a hyperarid coastal region (AI < 0.05) and a central arid region (0.05 ≤ AI < 0.2) [5, 6] (Figure 1A). Despite receiving extremely low annual rainfall, the hyperarid coastal zone experiences frequent fog events, approximately 3–9 days/month, which decrease in frequency and duration beyond 60 km inland [2, 4, 7].

Considering the minimal precipitation along the hyperarid coast, fog-derived moisture has been proposed as the dominant source of bioavailable water for these soil microbial communities [3, 8-10]. Fog inputs are estimated to contribute up to 183 mm deposited moisture annually [2, 4, 7], and contribute to slight increases in sub-surface (0–5 cm) soil relative humidity, compared to soils from rainfall-dominated zones [3]. However, their limited capacity to penetrate the desert pavement and enter the root zone restricts microbial and plant productivity [1, 7]. Consequently, soil organic matter, nitrogen and carbon content are lower in the hyperarid compared to the arid inland region [3, 11, 12]. High soil ionic content from marine aerosol deposition in the coastal region may further limit the bioavailability of fog-derived moisture [12]. While it is clear that fog is a strong driver of lichen and biological soil crust development [8, 13, 14], there has been extensive debate over the role of fog-derived water in supporting the sub-surface soil microbiome [10, 12, 15, 16].

72 ***Microbial trace gas oxidation and alternative survival strategies in dryland environments***

73 It is well-established that the majority of microbial growth and metabolic processes cease at
74 water activities (a_w) < 0.9, whilst limited function at water activities as low as 0.3 a_w occurs
75 in some specialist taxa [17-20]. The Namib Desert is an environment under severe water
76 stress, with average immediate sub-surface (1–2 cm) soil water activities < 0.5 a_w [3]. Despite
77 this stress, diverse and metabolically active microbial communities persist within both
78 surface and shallow sub-surface soils [12, 20-23]. It is estimated that over 95% of soil
79 microorganisms exist in slow-growing or dormant states [24, 25], particularly during
80 desiccation stress [19]. Microbial dormancy followed by rapid resuscitation during wetting
81 has been proposed as a key survival strategy in dryland ecosystems including the Namib
82 Desert [22, 26-28].

83 Microbial trace gas oxidation is increasingly recognised as a generalist strategy to support
84 persistence in both hot and cold desert ecosystems [27, 29-32]. In particular, molecular
85 hydrogen (H_2) is a ubiquitous and energetically favourable substrate present at ~530 ppbv
86 throughout the atmosphere, capable of readily diffusing through soil surface layers and cell
87 membranes [27, 30, 33]. In some hyperarid environments, rapid H_2 uptake and the presence
88 of abundant high-affinity hydrogenases has led to the hypothesis that energy derived from
89 hydrogen oxidation may exceed requirements for cell maintenance, supporting microbial
90 growth via carbon fixation pathways [34-37]. This process, termed atmospheric
91 chemosynthesis, may complement or even surpass photoautotrophic primary production in
92 water-restricted environments with low phototroph abundances. Atmospheric chemosynthesis
93 has been established as a significant contributor to microbial carbon fixation in polar soils
94 [34, 36]. However, microbial trace gas oxidation and its potential contribution to carbon
95 fixation is poorly characterised in hot deserts, particularly in desiccated soils [31, 38].

96 In this pilot study, the impact of water limitation and regime on microbial atmospheric
97 hydrogen oxidation activity was investigated in desiccated and wetted soils, across a
98 longitudinal aridity gradient in the Namib Desert. The inverse distribution of fog and rainfall-
99 dominated water regimes across the coastal and inland regions of this gradient are proposed
100 to drive divergent microbial community composition and function. Trace gas chemotrophy is
101 predicted to support shallow sub-surface microbial communities in these severely water-
102 limited soils, particularly in the hyperarid coastal zone receiving low-volume fog inputs.

103

104 ***Materials and Methods***

105 ***Soil sampling across the Namib Desert C14 aridity transect***

106 Ten sites were sampled across a 200 km longitudinal aridity transect, referred to henceforth
107 as the C14 transect, spaced at 20 km intervals across a well-defined west-east aridity gradient
108 from the coastal to inland margins of the Namib Desert (Figure 1B). The C14 transect and
109 surrounding soils are divided into three well-defined xeric zones: the "Fog zone" (coastal
110 sites 2–6), "Hyperarid zone" (central sites 8–14) and "Arid zone" (inland sites 16–20). These
111 zones, proposed by Scola et al. (2018) [12], are supported by extensive research on soil
112 physicochemical parameters [11, 12, 16, 39, 40], rainfall, fog and humidity records [2-4, 11,
113 12, 16, 39], and microbial community analysis [12, 39, 40].

114 Duplicate (approx. 45 g) shallow sub-surface (1–5 cm) soil samples were aseptically
115 collected into sterile 50 mL tubes from the ten C14 transect sites in April 2023 (Figure 1B,
116 Table 1). Samples were immediately stored at 4 °C after sampling and transported to the
117 Centre for Microbial Ecology and Genomics (CMEG, Pretoria, South Africa), where they
118 were stored at 4 °C until shipment. Samples were imported to the University of New South
119 Wales (NSW, Australia), where half of the bulk soil from each site was stored at -80 °C and

the remaining soil stored at 4 °C until use. Soil samples used for hydrogen oxidation and respiratory burst microcosm assays were stored at 4 °C, while DNA extraction and all other analysis was conducted on soils stored at -80 °C.

Soil moisture analysis

Soil moisture content (SMC%) was calculated using the gravimetric oven-drying method [41]. Triplicate 1.5 g soil subsamples from each site were placed into pre-weighed 20 mL glass vials and oven-dried at 105 °C for 48 h. Sample vials were removed from the oven and cooled to RT in a gas-tight container with silica beads (Ajax Finechem) before re-weighing using an analytical balance (Sartorius AG). SMC% was recorded by calculating the mass of water loss after drying as a percentage of the dry soil weight.

Aridity Index (AI) data for each site was retrieved from the Global Aridity Index and Potential Evapotranspiration Database (Version 3) [6]. Soil water potential and water activity was calculated from previously published datasets that used iButton remote sensing data to record sub-surface soil temperature and relative humidity along the C14 transect [3]. Sub-surface (0–10 cm) soil moisture content was retrieved from the FLDAS Noah Land Surface Model L4 Global Monthly 0.1° × 0.1° dataset [42], subset to a 30-year monthly climatic mean using NASA GES DISC by selecting the SoilMoi00_10cm_tavg variable between 1994–2024. Average annual rainfall data from each site was retrieved from a previously published dataset across the C14 transect [12].

141 ***Soil physicochemical parameters***

142 Total soil carbon (TC), organic carbon (TOC), inorganic carbon (TIC), nitrogen (N),
143 hydrogen (H) and sulfur (S) analysis was performed at the Mark Wainwright Analytical
144 Centre (MWAC, UNSW Sydney, Australia). Duplicate 0.25 g soil samples from each transect
145 site were first passed through a 0.15 mm sieve, and soil particles between 0.15–2 mm were
146 finely ground to < 0.15 mm using a mortar and pestle. Ground soil samples were then oven-
147 dried at 45 °C until constant mass (> 72 h). To quantify TOC, two additional soil samples per
148 site were dried and ground according to the same procedure. Inorganic carbonates were
149 removed by acidification with 1 M HCl, added gradually in excess, and incubated in glass
150 vials at RT for 12 h [43]. Acidified samples were washed with 90 mL sterile deionised water
151 and dried at 45 °C until constant mass (> 120 h). Soil mass loss after acidification was
152 recorded using an analytical balance (Sartorius AG), and TOC was calculated as a percentage
153 of total soil mass. CHNS analysis was performed on all samples via combustion at 1150 °C
154 using a varioMACRO CUBE elemental analyser (Elementar, Germany). TIC was calculated
155 as the difference between TC and TOC content.

156 Soil pH was measured using 2.5 g soil slurries at a 1:2.5 soil:deionised water ratio, with a pH
157 meter (HI12303, Hanna Instruments). Additional physicochemical parameters at C14 transect
158 sites have been investigated previously [12, 40].

159

160 ***Microbial community activity metrics***

161 *Intracellular ATP luminescence assay*

162 The BacTiter-Glo™ Microbial Viability Assay kit (Promega) was used to measure
163 intracellular ATP concentrations in C14 transect soil samples using a modified method
164 optimised for soils [44]. In triplicate, 1 g soil subsamples from each site were added to 4 mL

165 0.85% NaCl in 15 mL tubes and vortexed at maximum speed for 5 min to produce a soil
166 slurry. Slurry samples were then centrifuged at 180 rcf for 5 min and the supernatant was
167 collected. Triplicate 100 µL volumes of supernatant were used to perform the assay in 96-
168 well white luminescence plates (Greiner), according to manufacturer's instructions. A
169 standard curve was produced by serial dilution of 100 mM ATP solution (Thermo Fisher
170 Scientific). Background adjusted luminescence values were recorded using a CLARIOstar
171 Plus Microplate reader (BMG Labtech), and calculations were performed in MARS Data
172 Analysis Software v5.02 R3 (BMG Labtech).

173 *Respiratory activity assay in dry and wetted soils*

174 Basal respiration in dry soils and respiratory burst after wetting were recorded over 14 days
175 using a custom-built CO_2 and O_2 respirometry system (Qubit Systems, Canada). Triplicate 1
176 g subsamples of C14 transect soils stored at 4 °C were placed into sterile 114 mL glass vials
177 (Glass Vials Australia, NSW) and equilibrated at RT for three days. Following equilibration,
178 soil microcosms were sealed using gas-tight butyl rubber stoppers (Glass Vials Australia,
179 NSW) and incubated in the dark at 30 °C. Heat-killed controls were prepared from each site
180 using 1 g soil autoclaved at 121 °C for 15 min.

181 Headspace CO_2 and O_2 was measured at five timepoints (0, 24, 56, 120, 144 and 168 h) over
182 the one-week basal incubation period. A gas-tight syringe (Trajan Scientific) was used to
183 subsample 1 mL headspace gas from serum vial microcosms. Headspace subsamples were
184 injected through a gas-tight sample port at approximately 100 µL/s into 99.999% N_2 carrier
185 gas (Coregas, Australia). Using a Q-P103 Gas Pump (Qubit Systems), carrier and sample
186 gases were pumped through a Q-S151 Infrared CO2 analyser and Q-S102 O2 analyser (Qubit
187 Systems) at a constant rate. Flow rate was recorded via a Q-G266 Flow Monitor (Qubit
188 Systems). All readings were recorded using LabQuest Mini sensor data interfaces (Qubit

189 Systems) and headspace CO_2 and O_2 concentrations were calculated via the Logger Pro
190 v3.16.2 software.

191 After one week, each soil microcosm was wetted to approximately 50% water holding
192 capacity, estimated using the filter paper method [45]. Starting headspace CO_2 concentrations
193 were recorded immediately before wetting, as above, and wetted microcosms were incubated
194 under the same conditions. Repeat measurements were taken after 0.5, 1, 3, 5, 9, 24, 48 and
195 168 h. The cumulative respiratory burst was calculated for each site and timepoint by
196 normalising against the initial headspace CO_2 concentration.

197

198 ***Hydrogen oxidation rates in wet and dry soil microcosms***

199 For dry microcosm H_2 oxidation assays, five biological replicate soil subsamples (2 g) and a
200 heat-killed control (2 g soil autoclaved at 121 °C for 15 min) were prepared from each site,
201 along with an empty serum vial negative control. Microcosm H_2 oxidation activity was
202 recorded using gas chromatography as described previously [34, 36]. All soil samples and
203 controls were placed into sterile 114 mL serum vials sealed with gas-tight butyl rubber
204 stoppers and incubated in the dark at 30 °C. Sterile H_2 gas in synthetic air-balance (BOC,
205 Australia) was injected into the headspace of each serum vial microcosm to achieve a final
206 headspace concentration of 10,000 ppbv. Headspace gas from each microcosm was
207 subsampled in 1 mL volumes at regular intervals using a gas-tight syringe (Trajan Scientific)
208 and H_2 concentration was measured using a Peak Performer 1 Gas Analyser (Peak
209 Laboratories, USA). For H_2 oxidation analysis in wet soil microcosms, the same procedure
210 was repeated using five additional 2 g soil subsamples from each site, wetted immediately
211 prior to gas addition using 400 µL sterile ddH_2O equilibrated to 30 °C.

212 Sub-atmospheric hydrogen oxidation was confirmed after two consecutive headspace H_2
213 readings < 530 ppbv. First order rate constants (*k*) were calculated using linear regression (R^2
214 > 0.9). Atmospheric hydrogen oxidation rates were calculated at headspace H_2 = 530 ppbv
215 with a total microcosm headspace volume of 114 mL at 30 °C and 1 atm. Rates were
216 normalised against total 16S rRNA gene copy numbers per gram soil.

217

218 ***DNA extraction and quantitative PCR***

219 Genomic DNA was extracted from quadruplicate 0.5 g bulk soil subsamples stored at -80 °C
220 from each site, using the FastDNA™ Spin Kit for Soil (MP Biomedicals), according to
221 manufacturer's instructions. Extracted DNA was eluted in 70 µL warm (60 °C) UltraPure™
222 DNase/RNase-free distilled water (Invitrogen) and stored at -80 °C. Quantity and purity of
223 extracted DNA was assessed using both Nanodrop (Thermo Fisher Scientific) and the
224 Qubit™ dsDNA High Sensitivity Assay (Thermo Fisher Scientific). To reduce PCR
225 inhibition, gDNA was further diluted in UltraPure™ DNase/RNase-Free distilled water
226 (Invitrogen) to produce final concentrations between 1.76–20.00 ng/µL.

227 Extracted gDNA was used for qPCR quantification of total bacterial abundance using the
228 universal 16S rRNA gene degenerate primer set Eub1048f/Eub1194r (Eub1048f; 5'-
229 GTGSTGCAYGGYTGTCGTCA, Eub1194r; 5'ACGTCRTCCMCACCTTCCTC) [46], as
230 described previously [47]. QPCR reaction mixtures were prepared using 10 µL QuantiNova
231 SYBR Green PCR Master Mix (Qiagen, Australia), 0.5 µL of each 40 µM forward and
232 reverse primer (Integrated DNA Technologies), 7 µL UltraPure™ DNase/RNase-free
233 distilled water (Invitrogen), 1 µL of 5 µg/mL T4 Gene 32 (New England Biolabs), and 1 µL
234 diluted template gDNA or positive control. A synthetically designed gene fragment (gBlocks;
235 Integrated DNA Technologies, Australia) containing a representative 16S rRNA gene

236 sequence (MF689012.1) was used to generate a standard curve over five orders of magnitude
237 [47]. All standards, samples and negative template control reactions were performed in
238 triplicate.

239 Reaction mixtures were added to 96-well thin wall PCR plates (Bio-Rad Laboratories) and
240 sealed using optically clear plate seals (Bio-Rad Laboratories). The thermocycling protocol
241 was completed using a CFX96 Touch™ Real-Time PCR Detection System (Bio-Rad
242 Laboratories). Plates were incubated at 95 °C for 5 min, followed by 38 cycles of 95 °C for
243 20 s and 60 °C for 50 s. Quantitative fluorescence data was spectrophotometrically collected
244 during the combined extension and annealing step. Following PCR amplification, a melt
245 curve was performed from 50–95 °C, with fluorescence data collected at 0.5 °C steps
246 throughout. Data analysis was conducted using CFX Manager software (Bio-Rad
247 Laboratories). Amplification specificity was confirmed by visual inspection of melt peaks.

248

249 ***16S rRNA gene amplicon sequencing of soil microbial communities***

250 Paired-end amplicon sequencing was performed on gDNA samples from all transect sites at
251 the Ramaciotti Centre for Genomics (UNSW, Australia). The barcoded primer pair 515F-
252 Y/806RB (515F-Y; 5'-GTGYCAGCMGCCGCGGTAA, 806RB; 5'-
253 GGACTACNVGGGTWTCTAAT) was used to amplify the V4 region of the 16S rRNA gene
254 using the Illumina MiSeq v2 platform [48, 49]. Raw reads were processed into amplicon
255 sequence variants (ASVs) with DADA2 v1.30.0 [50] in R v4.3.1. Reads with ambiguous
256 bases were discarded, and residual primer sequences were removed with cutadapt v4.3 [51].
257 Forward and reverse reads were quality filtered using the following parameters: reads
258 matching phiX removed, 2 maximum expected errors allowed, truncation length of 220 and
259 215 nt, minimum read length of 150 nt, and a read truncation quality threshold of 2. Paired

260 reads were merged with mergePairs() using default parameters and chimeric reads were
261 removed with the removeBimeraDenovo() function, using the consensus method. Taxonomy
262 was assigned to merged reads with the assignTaxonomy() command, implementing the RDP
263 Naive Bayesian Classifier algorithm [52] using SILVA database v138.1 [53]. Processed
264 ASVs assigned to mitochondria or chloroplasts were removed.

265 ASV sequences were aligned using MAFFT v7.526 [54], and an unrooted phylogenetic tree
266 was built using FastTree v2.1.11 [55] under the GTR+Gamma model [56]. The resulting tree
267 was utilised to calculate weighted UniFrac distance matrices [57] using phyloseq v1.46 [58].
268 Raw ASV abundance tables were rarefied to the minimum read count using phyloseq v1.46
269 [58]. Microbial community composition across C14 transect sites was analysed in vegan
270 v2.6-10 [59] using principal coordinates analysis (PCoA) based on weighted UniFrac
271 distances and the rarefied count table. Permutational ANOVA (PERMANOVA) was
272 performed using the adonis2 function in vegan v2.6-10 [59] with 999 permutations, where
273 each explanatory variable was tested individually against the weighted UniFrac dissimilarity
274 matrix.

275 Differentially abundant taxa were identified using Maaslin2 v1.16.0 [60] from rarefied data
276 aggregated to taxonomic level, excluding unclassified taxa. Linear regression models
277 (analysis method = “LM”) were used with default standardisation settings, and no
278 normalisation was applied. The Fog zone was specified as the reference group for
279 comparisons across xeric zones. The minimum non-zero prevalence threshold was set at 30%
280 and nominal p-values were adjusted via the Benjamini-Hochberg correction method to a
281 significance threshold of qval $\leq$ 0.20.

282

Data analysis and visualisation

All community activity and aridity datasets were analysed in RStudio [61] using R v4.3.1. Data processing was performed using reshape2 v1.4.4 [62], stringr v1.5.1 [63] and readr v2.1.5 [64]. Aridity Index datasets were processed and visualised using the terra v1.8.21 [65] and tidyterra v0.7.0 [66] packages. Statistical analysis was performed using dplyr v1.1.4 [67] and ggpubr v0.6.0 [68]. Correlation analysis was performed using corrplot v0.92 [69].

Mantel correlogram was calculated with vegan's v2.6-10 [59] mantel.correlog() function between the weighted UniFrac distance matrix and the geographical distances between sampling points. Geographical distances between sampling points were calculated from GPS coordinates using the Haversine method [70] as implemented in the geosphere package v1.5-20 [71]. Optimal number of bins for Mantel correlogram was calculated based on the Freedman-Diaconis rule [72] with the hist.FD() function from the MASS package v7.3-60 [73].

All other data visualisation was performed using ggplot2 v3.5.1 [74], patchwork v1.3.0 [75], pals v1.10 [76], tidyverse v2.0.0 [77] and ggtext v0.1.2 [78].

Results

Water availability and soil properties across the C14 transect

The Aridity Index (AI) of sites across the C14 transect increased from west to east, with the lowest recorded at Fog zone site C14-2 (AI = 0.0072), and the highest at Arid zone site C14-20 (AI = 0.0780) (Table 1). Sites C14-2 to C14-14, spanning the Fog and Hyperarid zones, were classed as hyperarid (AI < 0.05), and Arid zone sites C14-16–20 were classed as arid (0.05 ≤ AI < 0.2) [5].

Table 1: Soil moisture metrics and physicochemical properties of C14 transect sampling sites.

Site	Xeric zone [a]	Lat	Lon	Aridity Index (AI)	Gravimetric SMC%	Annual rainfall (mm)	Water potential (MPa)	Water activity (a_w)	Sub-surface SMC (m^3/m^3) [b]	TC%	TIC%	TOC%	N%	H%	S% [c]	pH
C14-2	F	-23.001	14.672	0.0072	1.53	16.7	-100.81	0.498	0.173	0.27	0.19	0.08	0.05	0.41	2.32	6.70
C14-4	F	-23.018	14.860	0.0112	0.20	21.5	-123.47	0.432	0.182	0.18	0.14	0.04	0.04	0.06	0.08	7.19
C14-6	F	-23.066	15.040	0.0196	0.82	40	-144.38	0.384	0.169	0.63	0.55	0.08	0.03	0.26	0.39	6.91
C14-8	HA	-23.143	15.209	0.0233	0.23	59	-162.43	0.333	0.163	0.16	0.11	0.05	0.04	0.09	0.07	7.03
C14-10	HA	-23.246	15.360	0.0308	0.81	62	-162.02	0.346	0.163	1.03	0.89	0.14	0.05	0.30	0.01	8.05
C14-12	HA	-23.311	15.534	0.0426	0.42	78.8	-184.07	0.312	0.162	0.38	0.18	0.20	0.07	0.26	nd	7.87
C14-14	HA	-23.325	15.715	0.0456	0.49	100.5	-145.68	0.384	0.163	1.05	0.83	0.22	0.05	0.27	nd	7.53
C14-16	A	-23.321	15.862	0.0532	0.35	133	-207.39	0.269	0.166	1.13	0.87	0.25	0.08	0.24	nd	7.71
C14-18	A	-23.345	16.011	0.0644	0.27	169.3	-231.39	0.230	0.170	0.22	0.04	0.18	0.06	0.17	nd	8.45
C14-20	A	-23.245	16.143	0.0780	0.31	184.8	-204.08	0.288	0.178	0.74	0.10	0.64	0.09	0.33	0.18	7.45

[a] *Xeric zonation is denoted as F = Fog zone, HA = Hyperarid zone, A = Arid zone*
[b] *Sub-surface (0–10 cm) soil moisture content*
[c] *nd denotes sulfur content not detected*

309

310 Gravimetric SMC% varied across the transect, ranging from 0.20–1.53% (0.54% ± 0.42%,
311 mean ± SD) (Table 1, Table S1). Average SMC% was highest in the Fog zone (0.85% ±
312 0.59%) followed by the Hyperarid (0.49% ± 0.25%) and Arid (0.31% ± 0.10%) zones.
313 Average water potential and a_w were highest in the Fog zone (water potential = -122.89 ±
314 17.79 MPa; a_w = 0.438 ± 0.047), followed by the Hyperarid (water potential = -163.55 ±
315 13.64 MPa; a_w = 0.344 ± 0.026) and Arid (water potential = -214.28 ± 12.17 MPa; a_w = 0.262
316 ± 0.024) zones. AI and rainfall were both negatively correlated with water potential ($p \leq$
317 0.001) and a_w ($p \leq 0.01$) (Figure S1). Gravimetric SMC% was positively correlated with a_w (ρ
318 = 0.67, $p \leq 0.05$). Sub-surface (0-10 cm) soil moisture content was not significantly
319 correlated with any other moisture metric ($p > 0.05$).

320 Soil pH ranged from slightly acidic to alkaline (6.70–8.45) and was highest in the Arid zone
321 (7.87 ± 0.42, mean ± SD), followed by the Hyperarid (7.62 ± 0.39) and Fog (6.93 ± 0.20)
322 zones (Table 1). Total carbon (TC) content was low (0.16–1.13%) across the transect, and
323 inorganic carbon (TIC) represented the majority of soil carbon in all sites except C14-12, 18
324 and 20. Total nitrogen (N) and organic carbon (TOC) content were lowest in the Fog zone (N
325 = 0.04% ± 0.01%, TOC = 0.06% ± 0.02%) and increased in the Hyperarid (N = 0.05% ±
326 0.01%, TOC = 0.15% ± 0.07%) and Arid (N = 0.07% ± 0.01%, TOC = 0.36% ± 0.20%)
327 zones. TOC, N and pH were significantly ($p \leq 0.05$) lower in the Fog zone compared to the
328 rest of the transect and were significantly positively correlated with AI (Figure S1).

329 ***Microbial activity and abundance biomarkers across xeric zones***

330 Microbial activity and 16S rRNA gene abundances increased from west to east across the
331 Fog, Hyperarid and Arid zones of the C14 transect (Figure 2). Total 16S rRNA gene copy
332 numbers ranged from 3.82×10^5 g^{-1} soil at Fog site C14-2 to 3.10×10^7 g^{-1} soil at Arid site

333 C14-16 (Figure 2A, Table S2). Average 16S rRNA gene copy number increased significantly
334 ($p \leq 0.01$) between each xeric zone as AI and rainfall increased (Figure S2A). The lowest
335 average 16S rRNA gene abundance was observed in the Fog zone (1.04×10^6 copies g^{-1}),
336 increasing 9-fold in the Hyperarid zone (9.15×10^6 copies g^{-1}) and by an order of magnitude
337 in the Arid zone (2.36×10^7 copies g^{-1}).

338 Similarly, cumulative 24-hour respiratory burst values ranged from 23.6 ppmv CO_2 g^{-1} soil
339 (Hyperarid site C14-8) to 2891.0 ppmv CO_2 g^{-1} soil (Arid site C14-20) (Figure 2B, Table S3-
340 4) and increased significantly ($p \leq 0.05$) between each xeric zone (Figure S2B). The average
341 24-hour cumulative respiratory burst across the Fog, Hyperarid and Arid zones was 213.2,
342 532.1 and 2181.9 ppmv CO_2 g^{-1} soil, respectively. Intracellular ATP concentrations ranged
343 from 0.002 nmol g^{-1} soil at Fog site C14-6 to 0.071 nmol g^{-1} soil at Arid site C14-18 (Figure
344 2C, Table S5). Whilst Arid zone sites recorded significantly ($p \leq 0.01$) higher ATP
345 concentrations than Fog and Hyperarid zone sites, average ATP concentrations between the
346 Hyperarid and Fog zones were not significantly different ($p > 0.05$) (Figure S2C).

347 Within the Fog zone, average ATP concentrations in sites C14-2 and C14-4 were 15- and 4-
348 fold higher, respectively, compared to site C14-6. Aridity Index was significantly positively
349 correlated with total 16S rRNA gene copy numbers ($\rho = 0.83$, $p \leq 0.01$), intracellular ATP (ρ
350 $= 0.76$, $p \leq 0.05$) and 24 h respiratory burst ($\rho = 0.90$, $p \leq 0.001$) (Figure S1). Total 16S copy
351 numbers were significantly positively correlated with cumulative 24 h respiratory burst ($\rho =$
352 0.92, $p \leq 0.001$) but not intracellular ATP content ($p > 0.05$).

353

354 ***<u>Trace gas oxidation rates in Namib Desert soil microcosms</u>***

355 In dry soil microcosms, two Fog zone sites (C14-2 and C14-4) exhibited rapid H_2 oxidation
356 activity to sub-atmospheric (< 530 ppbv) levels (Figure 3A). The remaining dry microcosms

357 demonstrated slow H_2 oxidation that did not reach sub-atmospheric levels after 1,500 h (~2
358 months) (Figure S3A). In contrast, soil wetting resulted in immediate (< 30 min) and rapid H_2
359 oxidation activity across all ten transect sites (Figure S3B), with sub-atmospheric hydrogen
360 oxidation activity observed in all moisture-stimulated microcosms (Figure 3B).

361 At atmospheric headspace H_2 concentrations, dry soil microcosms from Fog sites C14-2 and
362 C14-4 oxidised hydrogen at average rates of 2.27×10^{-7} and 4.27×10^{-8} nmol h^{-1} 16S $copy^{-1}$,
363 respectively (Table S6). Both C14-2 and C14-4 microcosms carried out significantly ($p \leq$
364 0.0001) accelerated atmospheric H_2 oxidation rates following moisture stimulation,
365 increasing over 30-fold compared to dry microcosm rates (Figure S4). In contrast, all wet soil
366 microcosms demonstrated rapid atmospheric H_2 oxidation rates, ranging from 1.59×10^{-8}
367 nmol h^{-1} 16S $copy^{-1}$ at Arid site C14-18 to 9.39×10^{-6} nmol h^{-1} 16S $copy^{-1}$ at Fog site C14-2
368 (Figure 3B, Table S7). In moisture-stimulated microcosms, the fastest H_2 oxidation rates were
369 observed in Fog zone soils (average = 3.55×10^{-6} nmol h^{-1} 16S $copy^{-1}$), while atmospheric H_2
370 oxidation rates decreased significantly ($p \leq 0.0001$) in the Hyperarid (3.84×10^{-8} nmol h^{-1}
371 16S $copy^{-1}$) and Arid (2.28×10^{-8} nmol h^{-1} 16S $copy^{-1}$) zones (Figure 3B).

372

373 ***<u>Microbial community composition along the Namib Desert C14 transect</u>***

374 Soils were dominated by the bacterial phyla *Actinobacteriota*, *Proteobacteria*, *Chloroflexi*
375 and *Bacteroidota*, and the archaeal phylum *Crenarchaeota*, together accounting for > 77.3%
376 of the microbial community (Figure 4A, Table S8). The relative abundance of
377 *Actinobacteriota* decreased significantly ($p \leq 0.001$) across the transect as AI increased
378 (Figure S6), decreasing from 42.3% in the Fog zone to 22.1% in the Arid zone (Figure 4A).
379 Conversely, the relative abundance of *Proteobacteria* increased significantly ($p \leq 0.005$)
380 from 11.5% in the Fog zone to 26.7% as the most abundant phylum in the Arid zone. The

five most abundant families were *Rubrobacteriaceae* (13.4%, *Actinobacteriota*), *Nitrososphaeraceae* (8.3%, *Crenarchaeota*), *Beijerinckiaceae* (7.7%, *Proteobacteria*), *Chloroflexi* family AKIW781 (4.9%) and *Geodermatophilaceae* (3.9%, *Actinobacteriota*) (Figure 4B).

PCoA ordination analysis explained 67.51% of total variance across the first two axes and showed clear seperation of microbial communities by xeric zone across the first axis (Figure 4C). Arid sites C14-16–20 clustered tightly, whereas Hyperarid sites C14-8–14 showed greater dispersal. Fog zone sites C14-2–6 exhibited the highest dispersion across both axes, indicating relatively higher compositional variability compared to the other zones. AI was the most significant ($p \leq 0.001$) explanatory variable, explaining 34.78% of variance in community structure (Table S9). Community composition was also significantly associated with rainfall ($p \leq 0.005$, $R^2 = 0.35$), nitrogen ($p \leq 0.01$, $R^2 = 0.29$), water potential ($p \leq 0.01$, $R^2 = 0.29$), pH ($p \leq 0.05$, $R^2 = 0.25$) and water activity ($p \leq 0.05$, $R^2 = 0.27$). The Mantel correlogram showed significant positive spatial autocorrelation ($r = 0.37$, $p < 0.01$) between sites up to approximately 20 km apart (i.e. immediately consecutive sites) (Figure S5). Between 20-60 km, correlations were weak ($r < 0.2$) and non-significant ($p > 0.05$), indicating that geographical distance alone does not explain community differences. At distances of ~110 km, sites were more dissimilar than expected by chance ($r = -0.33$, $p < 0.05$), while non-significant ($p > 0.5$) negative correlations were observed at all other distances.

In total, 129 taxa (13 phyla, 4 classes, 26 orders, 37 families and 49 genera) were significantly (qval ≤ 0.20) differentially abundant across xeric zones (Figure 5, Figure S7, Table S10). At the phylum level, the relative abundance of *Acidobacteriota*, *Abditibacteriota, Firmicutes*, *Proteobacteria, Bacteroidota* and *Crenarchaeota* increased significantly (qval ≤

405 0.20) in the Arid compared to the Fog zone. Similarly, seven phyla were enriched in the
406 Hyperarid zone relative to the Fog zone: *Entotheonellaeota, Firmicutes*, *Nitrospirota*,
407 *Acidobacteriota*, *Abditibacteriota*, *Armatimonadota* and *Crenarchaeota*. Conversely, the Fog
408 zone contained significantly (qval ≤ 0.20) greater relative abundances of *Gemmatimonadota*,
409 *Actinobacteriota*, *Deinococcota* and *Bdellovibrionota*.

410 Eight of the 12 families with total relative abundance ≥ 1.5% were significantly (qval ≤ 0.20)
411 differentially abundant between xeric zones (Figure 5). Of these, relative abundances of
412 *Chitinophagaceae, Geodermatophilaceae, Beijerinckiaceae* and *Pyrinomonadaceae* were
413 significantly (qval ≤ 0.20) greater within both the Arid and Hyperarid zones relative to the
414 Fog zone. In contrast, *Nitrososphaeraceae* were significantly more abundant in the Hyperarid
415 but not the Arid zone. Within the Fog zone, *Trueperaceae* were present at a greater relative
416 abundance compared to both other zones, while *Longimicrobiaceae* and *Rubrobacteriaceae*
417 had a greater relative abundance compared to the Hyperarid or Arid zone, respectively.

418 Across the transect, > 43.5% of ASVs remained unclassified at the genus level, with over half
419 of total ASVs unclassified in sites C14-4, C14-6 and C14-20 (Table S8). Seven classified
420 genera were significantly (qval ≤ 0.20) enriched in the Fog zone (Figure S7, Table S10). The
421 relative abundance of *Truepera, Oxalicibacterium* and *Amaricoccus* was greater in the Fog
422 zone relative to both other zones, while *Conexibacter,* Ellin6055 and *Lysobacter* were
423 enriched compared to the Hyperarid zone only, and *Rubrobacter* relative to the Arid zone. An
424 additional five genera were strongly differentially abundant (coef > 5.0), all enriched within
425 the Arid zone: *Flaviaesturariibacter, Planococcus, Edaphobaculum, Blastocatella* and
426 *Massilia*.

427

428 ## ***Discussion***

429 Differences in moisture regime and aridity across xeric zones of the Namib Desert are well-
430 established drivers of microbial community composition and function [12, 39, 40]. In this
431 pilot study, high-affinity H_2 oxidation and rapid resuscitation following soil wetting were
432 identified as key mechanisms likely to be supporting sub-surface soil microbial communities
433 across this aridity gradient. Dry soil microcosms from the hyperarid Fog zone exhibited rapid
434 hydrogen oxidation to sub-atmospheric concentrations without moisture stimulation (Figure
435 3A). In low-abundance Fog zone sites capable of H_2 oxidation in dry conditions, elevated
436 intracellular ATP concentrations compared to Fog zone site C14-6 were also observed,
437 providing evidence of a continuously active and strongly desiccation-resistant microbial
438 community.

439 ### ***Trace gas oxidation supports microbial communities in hyperarid Namib Desert soils***

440 Across the Namib Desert C14 transect, AI and average annual precipitation were highest in
441 the Arid zone (Table 1), with significantly ($p \leq 0.005$) higher total microbial abundances,
442 intracellular ATP and respiratory burst observed compared to the Hyperarid and Fog zones
443 (Figure 2, Figure S2). Despite this reduced biomass, dry soils from Fog zone sites C14-2 and
444 C14-4 demonstrated a remarkable capacity for rapid, high-affinity (530 ppbv) hydrogen
445 oxidation without water addition, at rates of 2.27×10^{-7} and 4.27×10^{-8} nmol h^{-1} 16S $copy^{-1}$,
446 respectively (Figure 3A). These rates exceed biomass-normalised H_2 oxidation rates recorded
447 in hyperarid Negev Desert soils by over two orders of magnitude [38], and contrast with
448 previous findings from hot desert soil studies where sub-atmospheric H_2 oxidation activity
449 was strongly limited in the absence of soil wetting [29, 31]. Although even faster atmospheric
450 H_2 oxidation rates have been recorded in Antarctic desert soils [34, 36], oxidation rates in
451 these Fog zone sites were comparable to those in cold, arid environments such as the high
452 Arctic [36] and Andean Altiplano [79], as well low-temperature Antarctic microcosms [35].

453 In these areas, energy derived from atmospheric hydrogen oxidation is predicted to sustain
454 microbial community biomass and potentially support hydrogenotrophic growth. Given the
455 extremely limited organic carbon availability (0.04–0.08%) and infrequent rainfall within the
456 Fog zone (Table 1) [3, 12], trace H_2 oxidation is likely to be a key contributor to cellular
457 energy requirements.

458 Higher soil moisture content and water potential within the Fog zone due to regular fog
459 inputs and humid coastal airflow [3] may have contributed to this unusual capacity for high-
460 affinity hydrogen oxidation in dry soils. However, these soils were severely water-restricted,
461 with average annual water availability < 0.5 a_w [3] and gravimetric SMC% as low as 0.20%
462 at site C14-4 (Table 1). Prior transcriptomic investigations on Namib Desert Fog zone soils
463 have revealed active transcription of genes associated with major metabolic pathways
464 including carbon and nitrogen assimilation, resuscitation and replication, even at
465 exceptionally low water activities (< 0.28 a_w) [20]. Furthermore, both Fog zone sites capable
466 of sub-atmospheric H_2 oxidation under dry conditions also exhibited elevated intracellular
467 ATP concentrations (Figure 2C), a known byproduct of hydrogen oxidation [80], compared
468 to Fog site C14-6. These findings support the growing body of evidence that some microbial
469 cells in hot desert soils retain significant metabolic functionality, including trace gas
470 oxidation, during severe desiccation [19].

471

472 ***Soil wetting results in rapid microbial resuscitation and hydrogen oxidation***

473 Rapid resuscitation following re-wetting is a dominant microbial survival strategy in global
474 dryland soils, with the majority of microbial growth restricted to short windows during
475 intermittent rain events [3, 22, 26, 28, 81]. In this study, moisture stimulation resulted in
476 immediate (< 30 min) H_2 uptake in soil microcosms from all Namib Desert C14 transect sites

477 (Figure S3B). In similar desiccated dryland samples, soil wetting has prompted rapid (< 15
478 min) resuscitation and upregulation of metabolic activity, including H_2 oxidation [26, 28, 31].
479 Consistent with observations of Australian and Negev Desert microcosms [26, 31, 38], soil
480 wetting significantly ($p < 0.0001$) increased hydrogen oxidation rates over 30-fold (Figure
481 S4) and resulted in sub-atmospheric H_2 oxidation activity in all microcosms (Figure 3B). In
482 wetted soil microcosms, biomass-adjusted H_2 oxidation rates were highest in Fog zone sites
483 and decreased significantly ($p < 0.01$) across xeric zones as aridity decreased (Figure 3B).
484 These findings support the hypothesis that trace gas oxidation is a survival strategy associated
485 with aridity and organic carbon limitation, complementing phototrophic and heterotrophic
486 growth in moisture-limited environments [38, 82]. Many *Actinobacteriota* regulate dormancy
487 and resuscitation of diverse bacterial lineages within the soil microbiome through the
488 production of extracellular resuscitation promoting factors (RPFs) [83, 84], and are also
489 implicated in trace gas oxidation [32]. The high relative abundance of *Actinobacteriota* taxa
490 across the transect (18.5–56.7%), particularly within the Fog zone (Figure 4A), may have
491 contributed to this rapid increase in H_2 oxidation activity after wetting.

492

493 ***Impact of water regime and availability on Namib Desert microbial community***
494 ***composition***

495 Water availability is a major driver of microbial abundance, diversity, and activity in
496 terrestrial environments, with the diversity and abundance of soil bacteria and fungi
497 decreasing as aridity increases [15, 19, 85, 86]. Photosynthetic growth is strongly dependent
498 on bioavailable water at minimum thresholds of 0.8–0.9 a_w, with *Cyanobacteria* particularly
499 inhibited by desiccation [9, 17]. Although *Cyanobacteria* have been identified as key taxa in
500 the hypolithic communities that colonise the underside of quartz rocks within the Namib

501 Desert, the relative abundances of these taxa are markedly reduced in open soils and biocrusts
502 [9, 23, 87]. This trend was reflected across the C14 transect, where *Cyanobacteria* comprised
503 0.2–4.7% of the total community (Figure 4A). Instead, sites were dominated by
504 *Actinobacteriota* (18.5–56.7%), *Proteobacteria* (8.2–30.6%) and *Chloroflexi* (6.5–27.5%)
505 lineages (Figure 4A). These metabolically flexible phyla have been linked with trace gas
506 oxidation and the genetic capacity for atmospheric chemosynthesis, and are proposed to
507 support primary production in water-limited environments [34-36, 38, 47].

508 Across the transect, the ratio between *Actinobacteriota* and *Proteobacteria* varied by xeric
509 zone, with *Actinobacteriota* significantly (qval ≤ 0.20) decreasing in relative abundance as AI
510 increased (Figure S6). In the Fog zone, *Actinobacteriota* were dominant (42.3% relative
511 abundance; Figure 4A), with *Rubrobacteriaceae* highly abundant across the transect (3.7–
512 21.7%, Figure 4B) and significantly enriched in the Fog zone at both the family and genus
513 (*Rubrobacter*) level (Figure 5, Figure S7, Table S10). *Rubrobacteriaceae* are associated with
514 strong resistance against UV radiation, desiccation, heat and oxidative stress, as well as
515 extensive DNA repair potential and mixotrophic growth strategies [26, 81, 88]. Furthermore,
516 *Rubrobacteriaceae* are key active taxa in global dryland soil microbial communities,
517 including in the Namib [20, 28], Negev [26, 81] and Atacama Deserts [86, 89]. High-affinity
518 oxygen-tolerant [NiFe]-hydrogenases have been identified in the genomes of dryland-
519 associated *Rubrobacteriaceae* [26, 36, 38, 81], and hydrogenase mRNA transcripts assigned
520 to *Rubrobacteriaceae* MAGs have been recovered from microcosms capable of trace H_2
521 oxidation under wet and dry conditions [26, 31]. In polar and hot deserts, *Rubrobacteriaceae*
522 are associated with mixotrophic growth due to the genetic capacity to use energy derived
523 from trace hydrogen oxidation and rhodopsin-based light harvesting to support persistence or
524 growth during starvation [35, 81]. Several other differentially abundant Fog zone taxa present
525 at lower relative abundances are also associated with hydrogen chemotrophy, including

526 *Conexibacter* (*Actinobacteria*) [36, 90], *Euzebyaceae* (*Actinobacteria*) [36, 91],
527 *Xanthomonadaceae* (*Proteobacteria*) [35, 36] and *Trueperaceae* (*Deinococcota*) [36]. These
528 hydrogenotrophic and desiccation resistant taxa, particularly the highly abundant
529 *Rubrobacteriaceae,* likely contribute to the significantly faster rates of H_2 oxidation observed
530 within the Fog zone.

531 In the Arid zone, the differentially abundant families *Beijerinckiaceae* (*Proteobacteria*) and
532 *Chitinophagaceae* (*Bacteroidota*) constituted > 20.9% of the microbial community (Figure 5,
533 Figure 4B). Within the dominant *Beijerinckiaceae* family, > 98.5% of classified ASVs were
534 assigned to two genera: *Microvirga* and *Psychroglaciecola* (Table S8). These heterotrophic
535 nitrogen-cycling genera are associated with bryophytes and rhizosphere root nodules across a
536 variety of arid environments, including the Namib Desert [21, 92-96]. Many *Microvirga*
537 species have the capacity to utilise plant-derived substrates for growth and synthesise plant-
538 growth promoting compounds [97-99] and have been identified as highly abundant in the
539 rhizosphere of Namib Desert plants such as *Sesuvium sesuvioides* and *Stipograstis* species
540 [21, 93]. Heterotrophic growth strategies may be more prevalent in the Arid zone compared
541 to fog-dominated areas due to the capacity of rainfall inputs to saturate soil and facilitate
542 dispersion of organic matter, as well as the higher TOC (0.18–0.64%) and N (0.06–0.09%)
543 content in the Arid zone (Table 1) [15]. The production of plant-growth promoting
544 compounds has also been reported in the differentially enriched Arid zone *Chitinophagaceae*
545 family, which are abundant within the rhizosphere of Namib Desert *Acanthosicyos horridus*
546 shrubs and are associated with degradation of plant-derived cellulose and chitin [100-102].
547 These microorganisms may contribute to supporting plant growth in the nutrient and moisture
548 limited Arid region of the Namib Desert.

549 Across the transect, a high proportion of ASVs belonged to unclassified clades, with > 26.9%
550 unclassified at the family level and > 43.6% at the genus level (Table S8). This high relative
551 abundance of "microbial dark matter" has been observed across global drylands [103],
552 representing a significant and underexplored microbial resource. Further research into these
553 uncharacterised taxa is recommended to support a greater understanding of the complex
554 microbially mediated processes within desert environments.

555 ***<u>Microbial hydro-genesis in Namib Desert sub-surface soils</u>***

556 Hydrogen oxidation, in addition to supporting energy requirements for basal cellular
557 metabolism [27, 33, 104], has been proposed to contribute to intracellular water production
558 through a process termed microbial hydro-genesis [15, 19, 35]. In this study, the
559 determination of substantial H_2 oxidation rates in dry soil microcosms, normalised against
560 cell numbers (estimated as 16S gene copies), allows for preliminary quantitative assessment
561 of intracellular water input derived from trace hydrogen oxidation.

562 Using the fastest H_2 oxidation rate determined in unwetted soil microcosm experiments (2.27
563 $\times 10^{-7}$ nmol h^{-1} 16S $copy^{-1}$, soil sample C14-2) (Figure 3A) and making the assumption that
564 cells contain single genomes and a single 16S gene copy per genome, we estimate H_2
565 oxidation (equimolar with H_2O production) to be 2.27×10^{-7} nmol h^{-1} $cell^{-1}$, equivalent to
566 4.09 fg H_2O produced h^{-1} $cell^{-1}$. Given a typical saturated cellular water content of 516 fg (for
567 *E. coli*, [105]), this contributes approximately 0.79% of total (saturated) cell water per hour.
568 In desiccated cells, such as those from site C14-4 (SMC% = 0.20%, a_w = 0.43; Table 1), this
569 contribution would be proportionally higher. While we acknowledge the multiple
570 assumptions built into this calculation, particularly those related to 16S gene copies and
571 cellular water contents, we argue that this calculated value of hydro-genesis derived from
572 atmospheric hydrogen oxidation in unwetted, low-moisture soils is significant, providing

support to the suggestion that this process contributes to cellular water budgets. This hydrogenic contribution, while unlikely to be functionally significant in water replete cells, may be vitally important to cellular function in moisture-limited environments [15, 19, 37].

Conclusions

In this study, the critical role of trace gas oxidation, particularly high-affinity hydrogen oxidation, in sustaining microbial communities in hyperarid Namib Desert soils is highlighted. Rapid sub-atmospheric H_2 oxidation activity in unwetted moisture-limited soils is proposed to contribute to cellular ATP and water budgets, supporting a continuously active desiccation resistant microbial community. In hyperarid, fog-dominated soils, taxa implicated in trace gas oxidation dominated, while heterotrophic taxa were differentially abundant within the Arid zone. Emerging evidence of interconnected phototrophic, heterotrophic and hydrogenotrophic growth strategies in hot and polar desert soils supports the need for broader studies that link water regime to functional capacity and primary production dynamics in these complex ecosystems.

Acknowledgements

This research was supported by an Australian Government Research Training Program (RTP) Scholarship awarded to DZT, the Australian Research Council (ARC) Discovery Project (DP240102658) awarded to BCF and a National Research Foundation of South Africa grant (137954) awarded to DAC. We thank the Gobabeb-Namib Research Institute (http://gobabeb.org/) in Namibia for their hospitality and field assistance. Field research was conducted under a research permit RPIV00112018, issued by the National Commission on Research, Science and Technology, and supported by the Ministry of Environment, Forestry

and Tourism in Namibia. This research includes computations using the computational cluster Katana supported by Research Technology Services at UNSW Sydney (DOI: 10.26190/669X-A286).

CRediT author contribution statement

DZT (Formal analysis, Investigation, Methodology, Visualisation, Writing – original draft, Writing – review & editing), **PHL** (Conceptualisation, Writing – review & editing), **XVC** (Formal analysis, Data curation, Visualisation, Writing – review & editing), **AER** (Methodology, Writing – review & editing), **TL** (Formal analysis, Methodology), **NMDL** (Formal analysis, Writing – review & editing), **GMK** (Project administration, Resources), **DAC** (Conceptualisation, Funding acquisition, Project administration, Resources, Supervision, Writing – review & editing), **BCF** (Conceptualisation, Funding acquisition, Project administration, Resources, Supervision, Writing – review & editing). All authors contributed to the final manuscript.

Conflicts of interest

The authors declare that they have no competing interests.

Data availability

Raw amplicon sequencing data are deposited upon publication in ENA under BioProject accession PRJEB97070. All remaining data generated or analysed during this study are included in this published article and its supplementary information files.

References

1. Seely MK. The namib dune desert: An unusual ecosystem. *Journal of Arid Environments*. 1978;**1**:117-28 https://doi.org/10.1016/S0140-1963(18)31736-1
2. Lancaster J, Lancaster, N., Seely M. Climate of the central namib desert. *Madoqua*. 1984;**1984**:5-61

3. Bosch J, Marais E, Maggs-Kölling G *et al.* Water inputs across the namib desert: Implications for dryland edaphic microbiology. *Frontiers of Biogeography*. 2022;**14** https://doi.org/10.21425/F5FBG55302
4. Eckardt FD, Soderberg K, Coop LJ *et al.* The nature of moisture at gobabeb, in the central namib desert. *Journal of Arid Environments*. 2013;**93**:7-19 https://doi.org/https://doi.org/10.1016/j.jaridenv.2012.01.011
5. United Nations Environment Programme. *World atlas of desertification: Second edition*, 1997.
6. Zomer RJ, Xu J, Trabucco A. Version 3 of the global aridity index and potential evapotranspiration database. *Sci Data*. 2022;**9**:409 https://doi.org/10.1038/s41597-022-01493-1
7. Mitchell D, Henschel JR, Hetem RS *et al.* Fog and fauna of the namib desert: Past and future. *Ecosphere*. 2020;**11** https://doi.org/10.1002/ecs2.2996
8. Büdel B, Darienko T, Deutschewitz K *et al.* Southern african biological soil crusts are ubiquitous and highly diverse in drylands, being restricted by rainfall frequency. *Microbial Ecology*. 2009;**57**:229-47 https://doi.org/10.1007/s00248-008-9449-9
9. Stomeo F, Valverde A, Pointing SB *et al.* Hypolithic and soil microbial community assembly along an aridity gradient in the namib desert. *Extremophiles*. 2013;**17**:329-37 https://doi.org/10.1007/s00792-013-0519-7
10. Warren-Rhodes KA, McKay CP, Boyle LN *et al.* Physical ecology of hypolithic communities in the central namib desert: The role of fog, rain, rock habitat, and light. *J Geophys Res-Biogeo*. 2013;**118(4)**:1451-60 https://doi.org/10.1002/jgrg.20117
11. Ramond JB, Woodborne S, Hall G *et al.* Namib desert primary productivity is driven by cryptic microbial community n-fixation. *Sci Rep-Uk*. 2018;**8** https://doi.org/10.1038/s41598-018-25078-4
12. Scola V, Ramond JB, Frossard A *et al.* Namib desert soil microbial community diversity, assembly, and function along a natural xeric gradient. *Microb Ecol*. 2017;**75**:193-203 https://doi.org/10.1007/s00248-017-1009-8
13. Lange OL, Green TGA, Meyer A *et al.* Water relations and carbon dioxide exchange of epiphytic lichens in the namib fog desert. *Flora*. 2007;**202**:479-87
14. Hinchliffe G, Bollard-Breen B, Cowan DA *et al.* Advanced photogrammetry to assess lichen colonization in the hyper-arid namib desert. *Front Microbiol*. 2017;**8**:2083 https://doi.org/10.3389/fmicb.2017.02083
15. Cowan DA, Cary SC, DiRuggiero J *et al.* 'Follow the water': Microbial water acquisition in desert soils. *Microorganisms*. 2023;**11** https://doi.org/10.3390/microorganisms11071670
16. Frossard A, Ramond JB, Seely M *et al.* Water regime history drives responses of soil namib desert microbial communities to wetting events. *Sci Rep*. 2015;**5**:12263 https://doi.org/10.1038/srep12263
17. Stevenson A, Burkhardt J, Cockell CS *et al.* Multiplication of microbes below 0.690 water activity: Implications for terrestrial and extraterrestrial life. *Environmental Microbiology*. 2015;**17**:257-77 https://doi.org/10.1111/1462-2920.12598
18. Williams JP, Hallsworth JE. Limits of life in hostile environments: No barriers to biosphere function? *Environ Microbiol*. 2009;**11**:3292-308 https://doi.org/10.1111/j.1462-2920.2009.02079.x
19. Bosch J, Varliero G, Hallsworth JE *et al.* Microbial anhydrobiosis. *Environ Microbiol*. 2021;**23**:6377-90 https://doi.org/10.1111/1462-2920.15699
20. León-Sobrino C, Ramond JB, Maggs-Kölling G *et al.* Nutrient acquisition, rather than stress response over diel cycles, drives microbial transcription in a hyper-arid namib

desert soil. *Frontiers in Microbiology*. 2019;**10** https://doi.org/10.3389/fmicb.2019.01054

21. Maphosa S, Steyn M, Lebre PH *et al.* Rhizosphere bacterial communities of namib desert plant species: Evidence of specialised plant-microbe associations. *Microbiol Res*. 2025;**293**:128076 https://doi.org/10.1016/j.micres.2025.128076
22. Armstrong A, Valverde A, Ramond JB *et al.* Temporal dynamics of hot desert microbial communities reveal structural and functional responses to water input. *Sci Rep-Uk*. 2016;**6**
23. Monus BD, Nghalipo EN, Marufu VJ *et al.* Contributions of hypolithic communities to surface soil organic carbon across a hyperarid-to-arid climate gradient. *Geoderma*. 2023;**433** https://doi.org/10.1016/j.geoderma.2023.116428
24. Blagodatskaya E, Kuzyakov Y. Active microorganisms in soil: Critical review of estimation criteria and approaches. *Soil Biology & Biochemistry*. 2013;**67**:192-211
25. Lennon JT, Jones SE. Microbial seed banks: The ecological and evolutionary implications of dormancy. *Nature reviews microbiology*. 2011;**9**:119-30
26. Imminger S, Meier DV, Schintlmeister A *et al.* Survival and rapid resuscitation permit limited productivity in desert microbial communities. *Nat Commun*. 2024;**15**:3056 https://doi.org/10.1038/s41467-024-46920-6
27. Leung PM, Bay SK, Meier DV *et al.* Energetic basis of microbial growth and persistence in desert ecosystems. *mSystems*. 2020;**5** https://doi.org/10.1128/mSystems.00495-19
28. Leon-Sobrino C, Ramond JB, Coclet C *et al.* Temporal dynamics of microbial transcription in wetted hyperarid desert soils. *FEMS Microbiol Ecol*. 2024;**100** https://doi.org/10.1093/femsec/fiae009
29. Bay SK, Dong X, Bradley JA *et al.* Trace gas oxidizers are widespread and active members of soil microbial communities. *Nat Microbiol*. 2021;**6**:246-56 https://doi.org/10.1038/s41564-020-00811-w
30. Greening C, Biswas A, Carere CR *et al.* Genomic and metagenomic surveys of hydrogenase distribution indicate h2 is a widely utilised energy source for microbial growth and survival. *ISME J*. 2016;**10**:761-77 https://doi.org/10.1038/ismej.2015.153
31. Jordaan K, Lappan R, Dong X *et al.* Hydrogen-oxidizing bacteria are abundant in desert soils and strongly stimulated by hydration. *mSystems*. 2020;**5** https://doi.org/10.1128/mSystems.01131-20
32. Lynch RC, Darcy JL, Kane NC *et al.* Metagenomic evidence for metabolism of trace atmospheric gases by high-elevation desert actinobacteria. *Frontiers in Microbiology*. 2014;**5** https://doi.org/10.3389/fmicb.2014.00698
33. Morita RY. Is h(2) the universal energy source for long-term survival? *Microb Ecol*. 1999;**38**:307-20 https://doi.org/10.1007/s002489901002
34. Ji M, Greening C, Vanwonterghem I *et al.* Atmospheric trace gases support primary production in antarctic desert surface soil. *Nature*. 2017;**552**:400-03 https://doi.org/10.1038/nature25014
35. Ortiz M, Leung PM, Shelley G *et al.* Multiple energy sources and metabolic strategies sustain microbial diversity in antarctic desert soils. *Proc Natl Acad Sci U S A*. 2021;**118** https://doi.org/10.1073/pnas.2025322118
36. Ray AE, Zaugg J, Benaud N *et al.* Atmospheric chemosynthesis is phylogenetically and geographically widespread and contributes significantly to carbon fixation throughout cold deserts. *Isme Journal*. 2022;**16**:2547-60 https://doi.org/10.1038/s41396-022-01298-5

37. Ray AE, Tribbia DZ, Cowan DA *et al.* Clearing the air: Unraveling past and guiding future research in atmospheric chemosynthesis. *Microbiol Mol Biol Rev*. 2023;**87**:e0004823 https://doi.org/10.1128/mmbr.00048-23
38. Bay SK, Waite DW, Dong X *et al.* Chemosynthetic and photosynthetic bacteria contribute differentially to primary production across a steep desert aridity gradient. *ISME J*. 2021;**15**:3339-56 https://doi.org/10.1038/s41396-021-01001-0
39. Naidoo Y, Valverde A, Pierneef RE *et al.* Differences in precipitation regime shape microbial community composition and functional potential in namib desert soils. *Microbial Ecology*. 2022;**83**:689-701 https://doi.org/10.1007/s00248-021-01785-w
40. Vikram S, Ramond JB, Ortiz M *et al.* Soil fungal diversity and assembly along a xeric stress gradient in the central namib desert. *Fungal Biol*. 2023;**127**:997-1003 https://doi.org/10.1016/j.funbio.2023.03.001
41. FAO. *Standard operating procedure for soil moisture content by gravimetric method*, Rome, 2023.
42. McNally A. Fldas noah land surface model l4 global monthly 0.1× 0.1 degree (merra-2 and chirps). Greenbelt, MD, USA.
43. He SF, Yang HY, Cui XQ. Technical note: Assessing pretreatment approaches for serial pyrolysis-oxidation analysis of sedimentary organic carbon. *Biogeosciences*. 2025;**22**:6243-53 https://doi.org/10.5194/bg-22-6243-2025
44. Dragone NB, Diaz MA, Hogg I *et al.* Exploring the boundaries of microbial habitability in soil. *J Geophys Res-Biogeo*. 2021;**126**:6052-52
45. Robertson GP. *Standard soil methods for long-term ecological research*, vol. 2: Oxford University Press, 1999.
46. Maeda H, Fujimoto C, Haruki Y *et al.* Quantitative real-time pcr using taqman and sybr green for actinobacillus actinomycetemcomitans, porphyromonas gingivalis, prevotella intermedia, tetq gene and total bacteria. *FEMS Immunology & Medical Microbiology*. 2003;**39**:81-86 https://doi.org/10.1016/s0928-8244(03)00224-4
47. Ray AE, Zhang E, Terauds A *et al.* Soil microbiomes with the genetic capacity for atmospheric chemosynthesis are widespread across the poles and are associated with moisture, carbon, and nitrogen limitation. *Front Microbiol*. 2020;**11**:1936 https://doi.org/10.3389/fmicb.2020.01936
48. Apprill A, McNally S, Parsons R *et al.* Minor revision to v4 region ssu rrna 806r gene primer greatly increases detection of sar11 bacterioplankton. *Aquatic Microbial Ecology*. 2015;**75**:129-37
49. Parada AE, Needham DM, Fuhrman JA. Every base matters: Assessing small subunit rrna primers for marine microbiomes with mock communities, time series and global field samples. *Environ Microbiol*. 2016;**18**:1403-14 https://doi.org/10.1111/1462-2920.13023
50. Callahan BJ, McMurdie PJ, Rosen MJ *et al.* Dada2: High-resolution sample inference from illumina amplicon data. *Nat Methods*. 2016;**13**:581-3 https://doi.org/10.1038/nmeth.3869
51. Martin M. Cutadapt removes adapter sequences from high-throughput sequencing reads. *2011*. 2011;**17**:3 https://doi.org/10.14806/ej.17.1.200
52. Wang Q, Garrity GM, Tiedje JM *et al.* Naive bayesian classifier for rapid assignment of rrna sequences into the new bacterial taxonomy. *Appl Environ Microbiol*. 2007;**73**:5261-7 https://doi.org/10.1128/AEM.00062-07
53. Quast C, Pruesse E, Yilmaz P *et al.* The silva ribosomal rna gene database project: Improved data processing and web-based tools. *Nucleic Acids Res*. 2013;**41**:D590-6 https://doi.org/10.1093/nar/gks1219

54. Katoh K, Standley DM. Mafft multiple sequence alignment software version 7: Improvements in performance and usability. *Molecular Biology and Evolution*. 2013;**30**:772-80 https://doi.org/10.1093/molbev/mst010
55. Price MN, Dehal PS, Arkin AP. Fasttree 2-approximately maximum-likelihood trees for large alignments. *Plos One*. 2010;**5** https://doi.org/10.1371/journal.pone.0009490
56. Tavaré S. Some probabilistic and statistical problems on the analysis of DNA sequences. *Lectures on Mathematics in the Life Sciences*. 1986;**17**:57-86
57. Lozupone CA, Hamady M, Kelley ST *et al.* Quantitative and qualitative β diversity measures lead to different insights into factors that structure microbial communities. *Appl Environ Microb*. 2007;**73**:1576-85 https://doi.org/10.1128/Aem.01996-06
58. McMurdie PJ, Holmes S. Phyloseq: An r package for reproducible interactive analysis and graphics of microbiome census data. *PLoS One*. 2013;**8**:e61217 https://doi.org/10.1371/journal.pone.0061217
59. Oksanen J, Simpson GL, Blanchet FG *et al.* Vegan: Community ecology package https://vegandevs.github.io/vegan/. 2025.
60. Mallick H, Rahnavard A, McIver LJ Multivariable association in population-scale meta-omics studies.
61. RStudio Team. Rstudio: Integrated development for r. RStudio, PBC, Boston, MA. http://www.rstudio.com/. 2020.
62. Wickham H. Reshaping data with the reshape package Journal of Statistical Software. Version 1.4.4 http://www.jstatsoft.org/v21/i12/. 2007.
63. Wickham H. Stringr: Simple, consistent wrappers for common string operations https://CRAN.R-project.org/package=stringr. 2023.
64. Wickham H, Hester J, Bryan J. Readr: Read rectangular text data https://CRAN.R-project.org/package=readr. 2024.
65. Hijmans RJ. Terra: Spatial data analysis https://rspatial.org/. 2024.
66. Hernangómez D. Using the tidyverse with terra objects: The tidyterra package. *Journal of Open Source Software*. 2023;**8**:5751 https://doi.org/10.21105/joss.05751
67. Wickham H, François R, Henry L *et al.* Dplyr: A grammar of data manipulation https://dplyr.tidyverse.org. 2023.
68. Kassambara A. Ggpubr: 'Ggplot2' based publication ready plots https://rpkgs.datanovia.com/ggpubr/. 2023.
69. Wei T, Simko V. R package 'corrplot': Visualisation of a correlation matrix Version Version 0.95 https://github.com/taiyun/corrplot. 2024.
70. Sinnott RW. Virtues of the haversine. *Sky Telescope*. 1984;**68**:159-59
71. Hijmans RJ. Geosphere: Spherical trigonometry https://github.com/rspatial/geosphere. 2024.
72. Freedman D, Diaconis P. On the histogram as a density estimator - l2 theory. *Z Wahrscheinlichkeit*. 1981;**57**:453-76 https://doi.org/Doi 10.1007/Bf01025868
73. Venables WN, Ripley BD. *Modern applied statistics with s*: Springer Science & Business Media, 2013.
74. Wickham H. Ggplot2: Elegant graphics for data analysis Springer-Verlag New York. https://ggplot2.tidyverse.org. 2016.
75. Lin Pedersen T. Patchwork: The composer of plots https://patchwork.data-imaginist.com. 2024.
76. Wright K. Pals: Color palettes, colormaps, and tools to evaluate them Version R package version 1.10 https://CRAN.R-project.org/package=pals. 2025.
77. Wickham H, Averick M, Bryan J *et al.* Welcome to the tidyverse. Journal of Open Source Software. 1686.

78. Wilke CO, Wiernik BM. Ggtext: Improved text rendering support for 'ggplot2' https://github.com/wilkelab/ggtext. 2025.
79. Garvin ZK, Abades SR, Trefault N *et al.* Prevalence of trace gas-oxidizing soil bacteria increases with radial distance from polloquere hot spring within a high-elevation andean cold desert. *ISME J*. 2024;**18** https://doi.org/10.1093/ismejo/wrae062
80. Soom S, Moning SU, Cook GM *et al.* Atp synthesis driven by atmospheric hydrogen concentrations. *Proc Natl Acad Sci U S A*. 2025;**122**:e2506353122 https://doi.org/10.1073/pnas.2506353122
81. Meier DV, Imminger S, Gillor O *et al.* Distribution of mixotrophy and desiccation survival mechanisms across microbial genomes in an arid biological soil crust community. *Msystems*. 2021;**6**:e00786-20 https://doi.org/10.1128/mSystems.00786-20
82. Li SY, Yang SS, Wei XM *et al.* Reduced trace gas oxidizers as a response to organic carbon availability linked to oligotrophs in desert fertile islands. *The ISME Journal*. 2023;**17**:1257-66 https://doi.org/10.1038/s41396-023-01437-6
83. Nikitushkin VD, Demina GR, Kaprelyants AS. Rpf proteins are the factors of reactivation of the dormant forms of actinobacteria. *Biochemistry (Mosc)*. 2016;**81**:1719-34 https://doi.org/10.1134/S0006297916130095
84. Lennon JT, Lehmkuhl BK, Chen L *et al.* Resuscitation-promoting factor (rpf) terminates dormancy among diverse soil bacteria. *mSystems*. 2025;**0**:e01517-24 https://doi.org/doi:10.1128/msystems.01517-24
85. Maestre FT, Delgado-Baquerizo M, Jeffries TC *et al.* Increasing aridity reduces soil microbial diversity and abundance in global drylands. *Proc Natl Acad Sci USA*. 2015;**112**:15684-9 https://doi.org/10.1073/pnas.1516684112
86. Schulze-Makuch D, Wagner D, Kounaves SP *et al.* Transitory microbial habitat in the hyperarid atacama desert. *P Natl Acad Sci USA*. 2018;**115**:2670-75 https://doi.org/10.1073/pnas.1714341115
87. Van Goethem MW, Makhalanyane TP, Cowan DA *et al.* Cyanobacteria and alphaproteobacteria may facilitate cooperative interactions in niche communities. *Front Microbiol*. 2017;**8**:2099 https://doi.org/10.3389/fmicb.2017.02099
88. Albuquerque L, Johnson MM, Schumann P *et al.* Description of two new thermophilic species of the genus rubrobacter, rubrobacter calidifluminis sp. Nov. And rubrobacter naiadicus sp. Nov., and emended description of the genus rubrobacter and the species rubrobacter bracarensis. *Syst Appl Microbiol*. 2014;**37**:235-43 https://doi.org/10.1016/j.syapm.2014.03.001
89. Bartholomaus A, Genderjahn S, Mangelsdorf K *et al.* Inside the atacama desert: Uncovering the living microbiome of an extreme environment. *Appl Environ Microbiol*. 2024;**90**:e0144324 https://doi.org/10.1128/aem.01443-24
90. Ortiz M, Leung PM, Shelley G *et al.* A genome compendium reveals diverse metabolic adaptations of antarctic soil microorganisms. *Preprint*. 2020 https://doi.org/10.1101/2020.08.06.239558
91. Mashamaite L, Lebre PH, Varliero G *et al.* Microbial diversity in antarctic dry valley soils across an altitudinal gradient. *Front Microbiol*. 2023;**14**:1203216 https://doi.org/10.3389/fmicb.2023.1203216
92. Cao W, Xiong Y, Zhao D *et al.* Bryophytes and the symbiotic microorganisms, the pioneers of vegetation restoration in karst rocky desertification areas in southwestern china. *Appl Microbiol Biotechnol*. 2020;**104**:873-91 https://doi.org/10.1007/s00253-019-10235-0

93. Marasco R, Mosqueira MJ, Fusi M *et al.* Rhizosheath microbial community assembly of sympatric desert speargrasses is independent of the plant host. *Microbiome*. 2018;**6**:215 https://doi.org/10.1186/s40168-018-0597-y
94. Yang Y, Liu WG, Huang TW *et al.* Similarities and differences in the rhizosphere biota among different ephemeral desert plants in gurbantunggut desert. *Environ Sci Eur*. 2023;**35** https://doi.org/10.1186/s12302-023-00724-5
95. Jara-Servin A, Silva A, Barajas H *et al.* Root microbiome diversity and structure of the sonoran desert buffelgrass (pennisetum ciliare l.). *Plos One*. 2023;**18** https://doi.org/10.1371/journal.pone.0285978
96. Lebre PH, Fouche J, Bosch J *et al.* Effects of fire intensity on soil microbial ecology in a grassland ecosystem. *Environmental Microbiology*. 2025;**27** https://doi.org/10.1111/1462-2920.70124
97. Msaddak A, Duran D, Rejili M *et al.* Diverse bacteria affiliated with the genera microvirga, phyllobacterium, and bradyrhizobium nodulate lupinus micranthus growing in soils of northern tunisia. *Appl Environ Microbiol*. 2017;**83** https://doi.org/10.1128/AEM.02820-16
98. Jimenez-Gomez A, Saati-Santamaria Z, Igual JM *et al.* Genome insights into the novel species microvirga brassicacearum, a rapeseed endophyte with biotechnological potential. *Microorganisms*. 2019;**7** https://doi.org/10.3390/microorganisms7090354
99. Ardley JK, Parker MA, De Meyer SE *et al.* Microvirga lupini sp. Nov., microvirga lotononidis sp. Nov. And microvirga zambiensis sp. Nov. Are alphaproteobacterial root-nodule bacteria that specifically nodulate and fix nitrogen with geographically and taxonomically separate legume hosts. *Int J Syst Evol Microbiol*. 2012;**62**:2579-88 https://doi.org/10.1099/ijs.0.035097-0
100. Unc A, Maggs-Kölling G, Marais E *et al.* Soil bacterial community associated with the dioecious acanthosicyos horridus in the namib desert. *Biol Fert Soils*. 2019;**55**:393-403 https://doi.org/10.1007/s00374-019-01358-7
101. Rosenberg E The family chitinophagaceae. In: Rosenberg E, DeLong EF, Lory S *et al.* (eds.). *The prokaryotes: Other major lineages of bacteria and the archaea*, Berlin, Heidelberg: Springer Berlin Heidelberg. 493-95. Retreived from https://doi.org/10.1007/978-3-642-38954-2_137
102. Kim HS, Kim JS, Suh MK *et al.* A novel plant growth-promoting rhizobacterium, rhizosphaericola mali gen. Nov., sp. Nov., isolated from healthy apple tree soil. *Sci Rep-Uk*. 2024;**14**:1038 https://doi.org/10.1038/s41598-024-51492-y
103. Li S, Lian WH, Han JR *et al.* Capturing the microbial dark matter in desert soils using culturomics-based metagenomics and high-resolution analysis. *NPJ Biofilms Microbiomes*. 2023;**9**:67 https://doi.org/10.1038/s41522-023-00439-8
104. Greening C, Carere CR, Rushton-Green R *et al.* Persistence of the dominant soil phylumacidobacteriaby trace gas scavenging. *Proceedings of the National Academy of Sciences*. 2015;**112**:10497-502 https://doi.org/10.1073/pnas.1508385112
105. Feijo Delgado F, Cermak N, Hecht VC *et al.* Intracellular water exchange for measuring the dry mass, water mass and changes in chemical composition of living cells. *PLoS One*. 2013;**8**:e67590 https://doi.org/10.1371/journal.pone.0067590

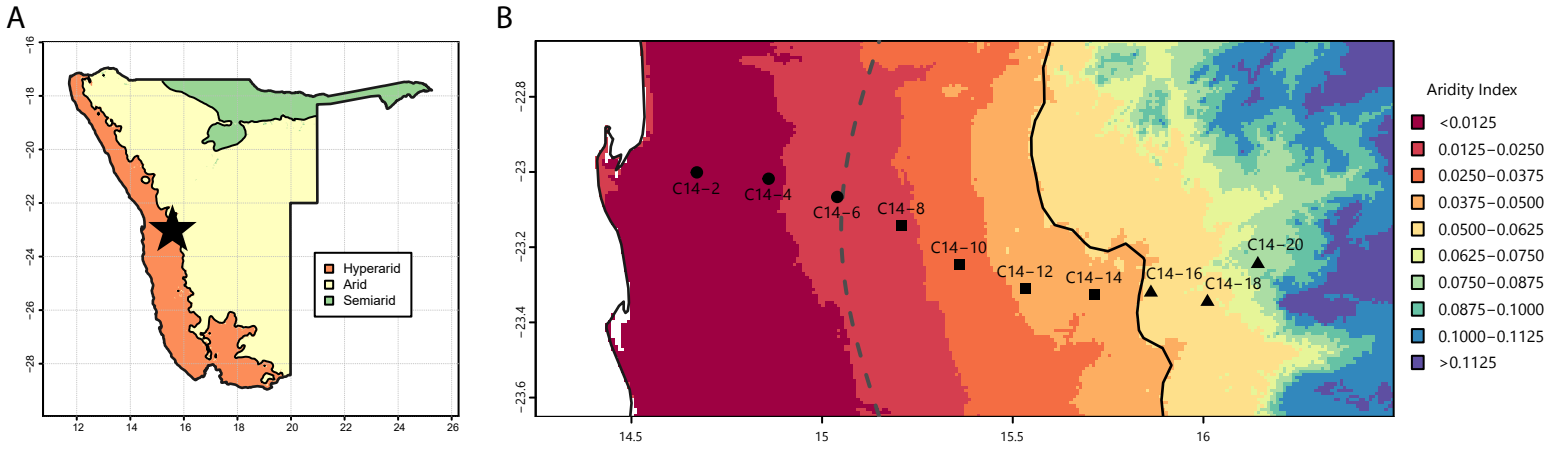

Figure 1: Aridity gradients of the Namib Desert and the C14 sampling transect *A) Xeric zonation of Namibia according to Aridity Index; transect location represented by the black star. B) GPS locations of ten sampling sites spaced 20 km apart along the 200 km C14 transect, located across a steep hyperarid-arid aridity gradient. The Fog zone is marked by the dotted grey line, and the hyperarid-arid boundary is marked by the solid black line. Fog, Hyperarid and Arid zone sites are indicated at circular, square and triangular points, respectively.*

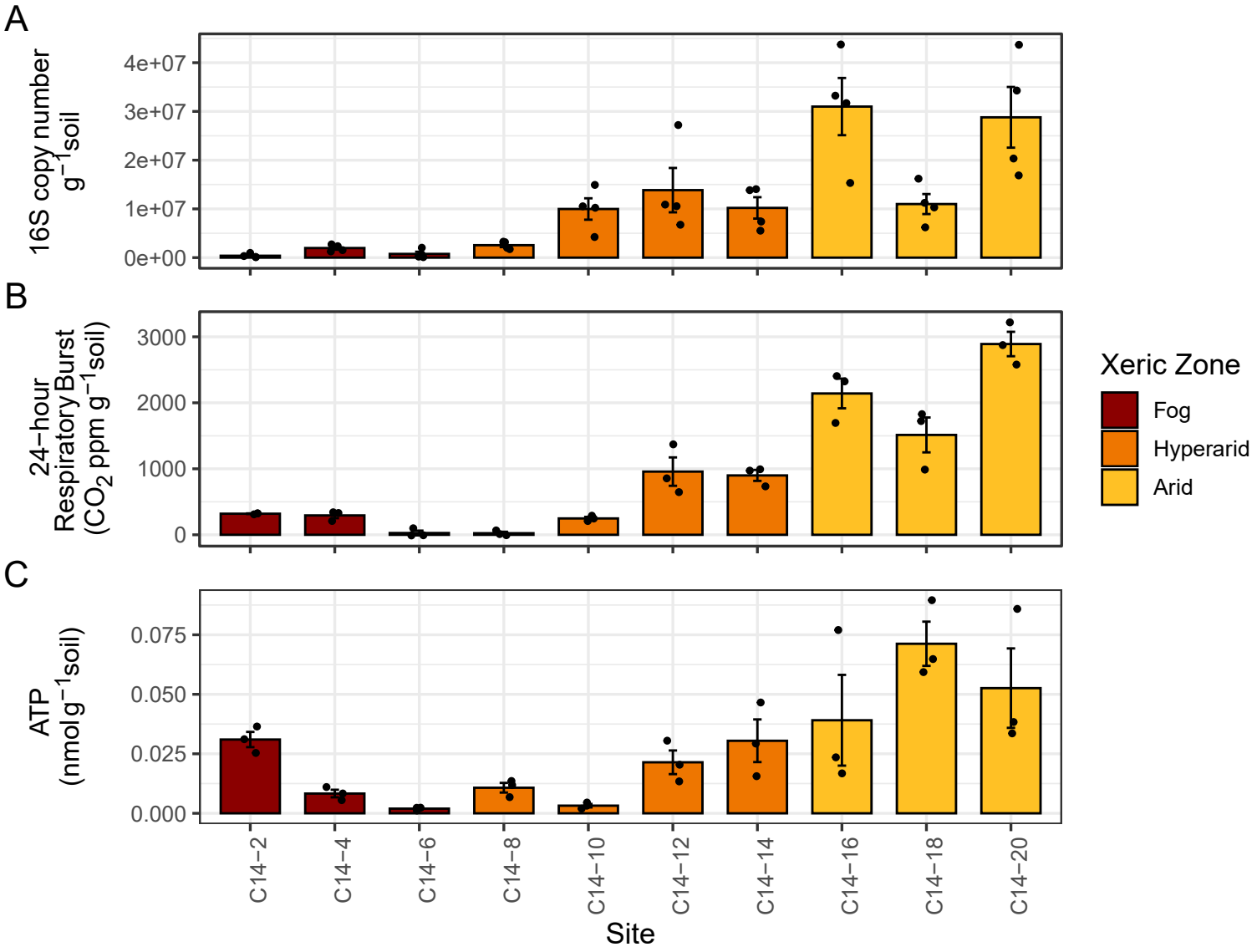

Figure 2: Soil microbial activity and abundances across the Namib Desert C14 transect. *Data points represent biological replicates (n=4 for A, n=3 for B and C) and error bars represent standard error. A) Total 16S rRNA gene copy numbers per site. Total copy number increased significantly ($p < 0.01$) between each xeric zone and was lowest in the Fog zone. B) Cumulative CO2 respiratory burst 24 h after moisture addition per site. Cumulative respiratory burst increased significantly ($p < 0.05$) between each xeric zone. B) Intracellular ATP concentrations per site. Average ATP was not significantly ($p > 0.05$) different between the Fog and Hyperarid zone.*

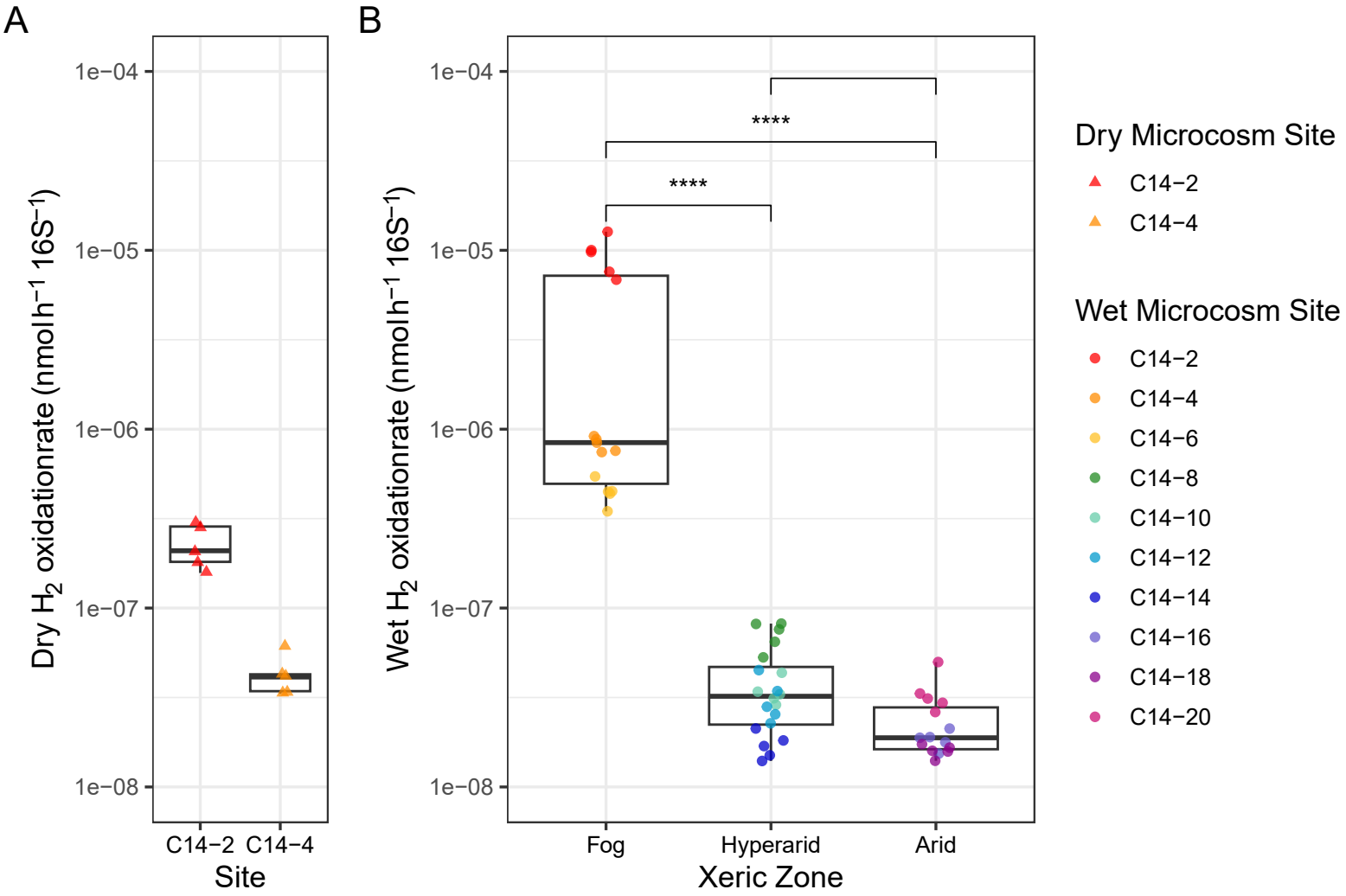

Figure 3: Atmospheric hydrogen oxidation rates in dry and wetted soil microcosms. *Rates were calculated at atmospheric hydrogen concentration = 530 ppbv and normalised to average 16S rRNA gene copy numbers per site. Significance thresholds were assigned as: $p \leq 0.05$ = *, $p \leq 0.01$ = **, $p \leq 0.001$ = ***, $p \leq 0.0001$ = ****. Data points shown represent n=5 biological replicates. A) Atmospheric H2 oxidation rates in dry soil microcosms from two Fog zone sites. All remaining dry soil microcosms did not oxidise hydrogen to below 530 ppbv after 1,500 hours. B) Atmospheric H2 oxidation rates in wetted microcosms.*

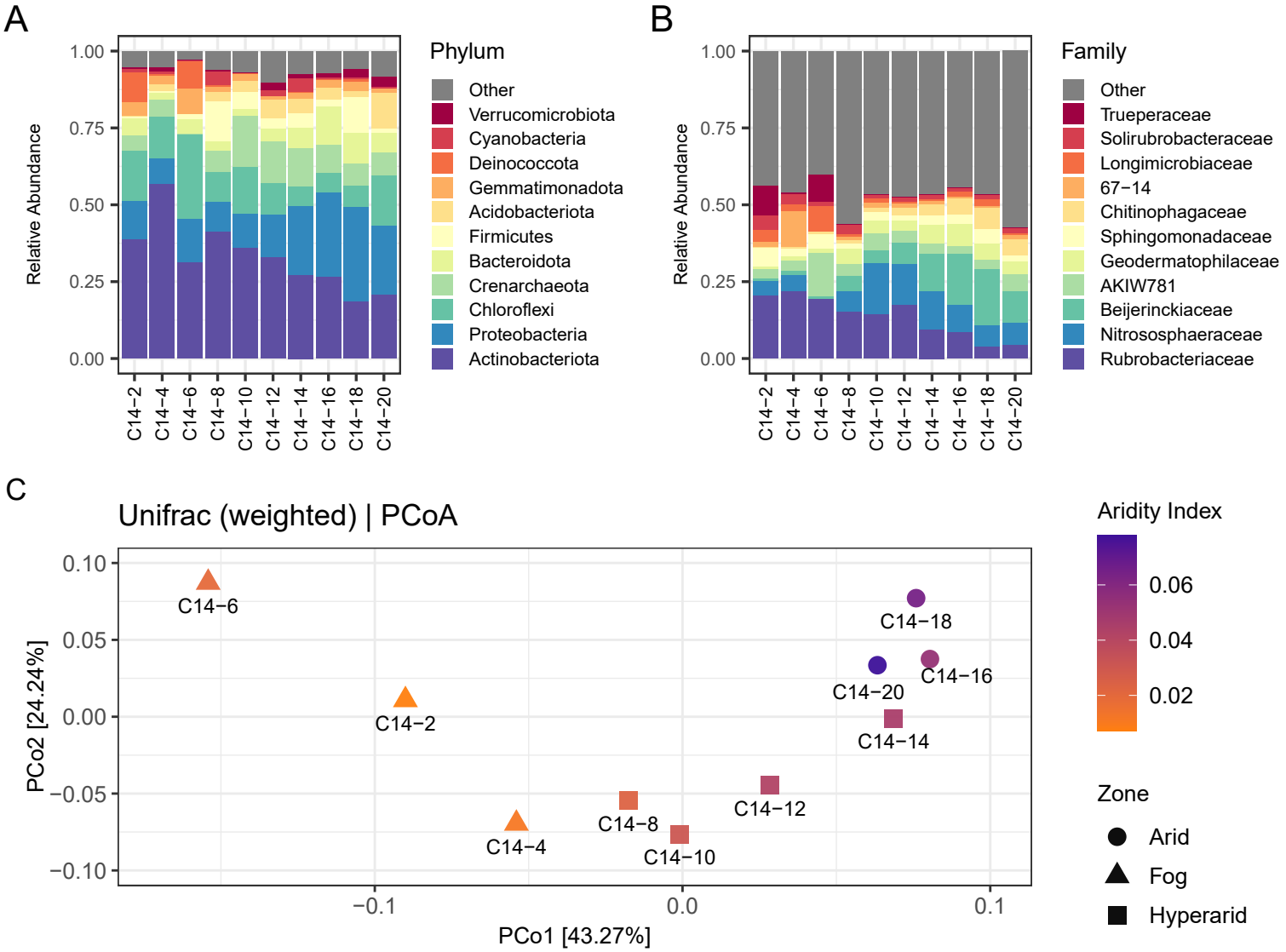

Figure 4: Bacterial and archaeal community composition and drivers across the Namib Desert C14 transect. *A) Relative community composition per site aggregated to phylum level. B) Relative community composition per site aggregated to family level. C) Principal coordinates analysis (PCoA) of microbial community composition based on weighted UniFrac distances. PCo1 and 2 explain 43.27% and 24.24% of total variance, respectively. Xeric zone is indicated by shape and transect sites are coloured according to Aridity Index (Table 1).*

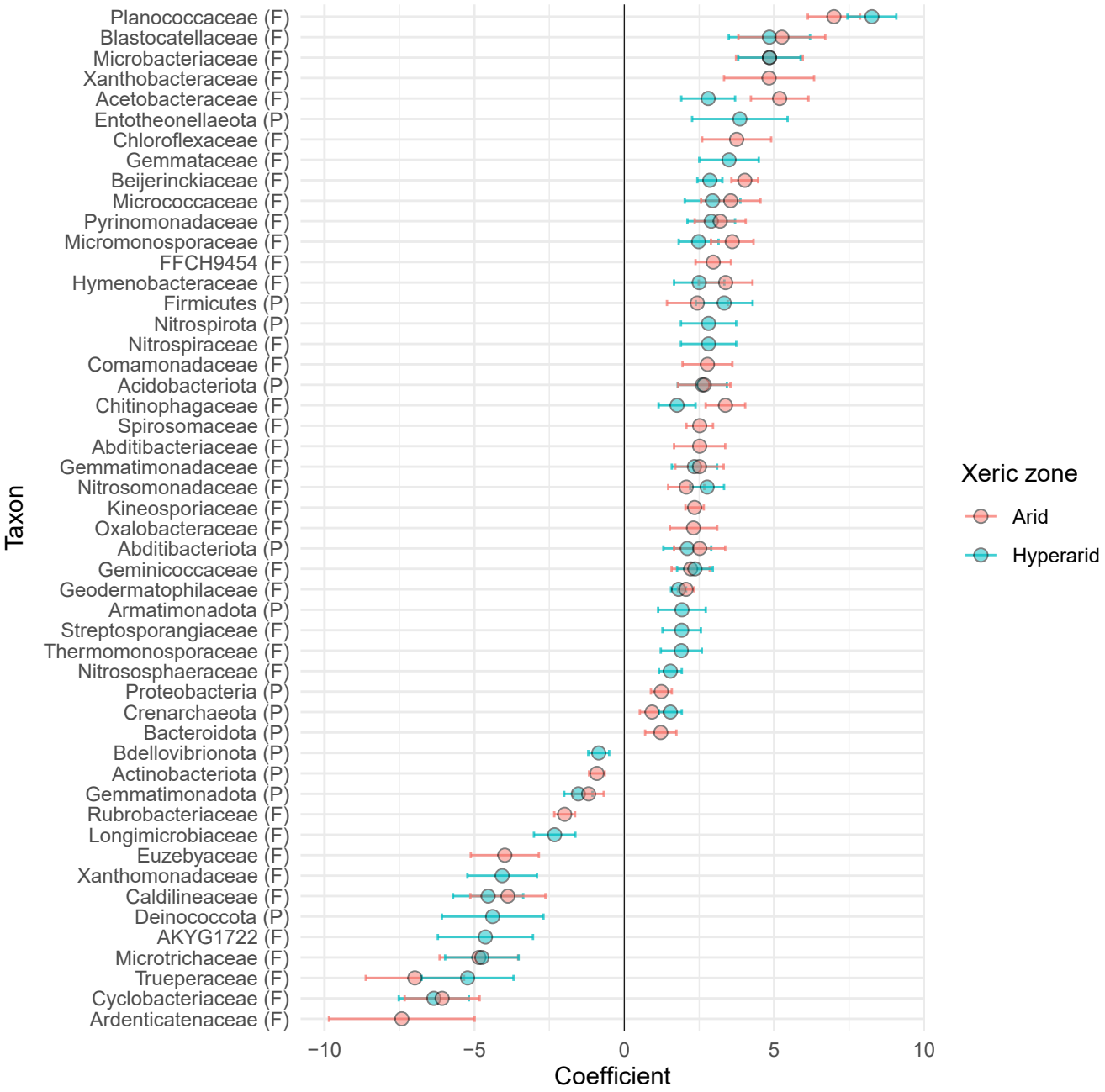

Figure 5: Differentially abundant taxa across xeric zones of a Namib Desert aridity transect, relative to the Fog zone. *Coefficient is a measure of the difference in relative abundance of taxa in Hyperarid and Arid zone sites, relative to Fog zone sites. Negative values indicate greater relative abundance within the Fog zone. Only coefficients with adjusted q-values ≤ 0.20 are shown. Error bars represent standard error. Taxonomic levels are represented as follows: (P) = phylum, (F) = family.*